Bulletin of the Seismological Society of America, Vol. 94, No. 2, pp. 760–768, April 2004

Simulation of the Planar Free Surface with Near-Surface Lateral Discontinuities in the Finite-Difference Modeling of Seismic Motion

by Peter Moczo, Jozef Kristek, and Martin Gális

Abstract Kristek *et al.* (2002) developed a technique for simulating the planar free surface in the 3D fourth-order staggered-grid finite-difference (FD) modeling of seismic motion. The technique is based on (1) explicit application of zero values of the stress-tensor components at the free surface and (2) adjusted FD approximations (AFDAs) to vertical derivatives at and near the free surface. The technique was shown to be more accurate and efficient than the standard stress-imaging technique in 1D models.

In this study, we tested accuracy of the AFDA technique in media with lateral material discontinuities reaching the free surface. We compared the FD synthetics with synthetics calculated by the standard finite-element (FE) method because the FE method naturally and sufficiently accurately satisfies the boundary conditions at the free surface and the traction interface continuity conditions at internal material discontinuities. The comparison showed a very good level of accuracy of the AFDA technique. We also demonstrated the very good sensitivity of our FD modeling to different positions of the same physical model in the spatial FD grid.

Introduction

The Earth's free surface, which in most seismological applications may be approximated by a surface with zero traction, strongly influences seismic motion. The finite-difference (FD) method has an inherent difficulty in implementing traction boundary conditions. Therefore, simulation of the traction-free condition is one of the key factors for the accuracy and efficiency of the FD modeling of seismic motion.

Here, we consider only simulation of the planar free surface in the staggered-grid FD schemes. In a Cartesian coordinate system (x_1, x_2, x_3), with the x_1 axis horizontal and positive to the right and the x_3 axis positive downward, consider a perfectly elastic isotropic half-space for $x_3 > 0$ with a planar free surface at $x_3 = 0$. Let $\rho(x_i)$; $i \in \{1,2,3\}$ be density, $\kappa(x_i)$ bulk modulus, $\mu(x_i)$ shear modulus, $\vec{\mathbf{u}}(x_i, t)$ displacement vector, t time, $\vec{\mathbf{f}}(x_i, t)$ body force per unit volume, and $\tau_{ij}(x_k, t)$ and $\varepsilon_{ij}(x_k,t)$; $i,j,k \in \{1,2,3\}$ stress and strain tensors. (Further, x_1, x_2, x_3 and x,y,z will be used interchangeably; similarly, 1, 2, 3 and x,y,z in the subscripts of the stress-tensor components and u_1, u_2, u_3 and u,v,w in referring to the displacement components.) The equation of motion and Hooke's law can be written as (summation convention for repeated subscripts assumed)

$$\rho\, \ddot{u}_i = \tau_{ij,j} + f_i \tag{1}$$

and

$$\tau_{ij} = \kappa\, \varepsilon_{kk}\delta_{ij} + 2\mu \left(\varepsilon_{ij} - \frac{1}{3}\, \varepsilon_{kk}\delta_{ij}\right), \tag{2}$$

where $\ddot{u}_i = \partial^2 u_i/\partial t^2$ and $\tau_{ij,j} = \partial\tau_{ij}/\partial x_j$. The traction vector $T_i(\vec{\mathbf{u}}, \vec{\mathbf{n}}) = \tau_{ji} n_j$ is equal to zero at the free surface at $z = 0$ with a unit normal vector $\vec{\mathbf{n}}(0,0,-1)$. Therefore,

$$\tau_{z\eta} = 0,\ \eta \in \{x,y,z\} \tag{3}$$

is the boundary condition at the free surface.

Equations (1) and (2) can be solved by an FD method. In the fourth-order staggered-grid FD schemes for interior grid points, the first spatial derivative of some function $\varphi(\xi)$ at $\xi = \xi_0$ is approximated by

$$\varphi_{,\xi}(\xi_0) = \frac{1}{h}\left\{a\left[\varphi\left(\xi_0 + \frac{3}{2}\, h\right) - \varphi\left(\xi_0 - \frac{3}{2}\, h\right)\right] + b\left[\varphi\left(\xi_0 + \frac{1}{2}\, h\right) - \varphi\left(\xi_0 - \frac{1}{2}\, h\right)\right]\right\}, \tag{4}$$

with $a = -1/24$, $b = 9/8$, and h being a grid spacing. An FD grid cell is shown in Figure 1. U and T_{xy} represent FD approximations to u (or, possibly, $\partial u/\partial t$) and τ_{xy}, and so on.

One natural option for localizing the planar free surface is the horizontal grid plane going through positions of the horizontal displacement components U, V, and stress-tensor components T_{xx}, T_{yy}, T_{zz}, and T_{xy}; for brevity, we will call it

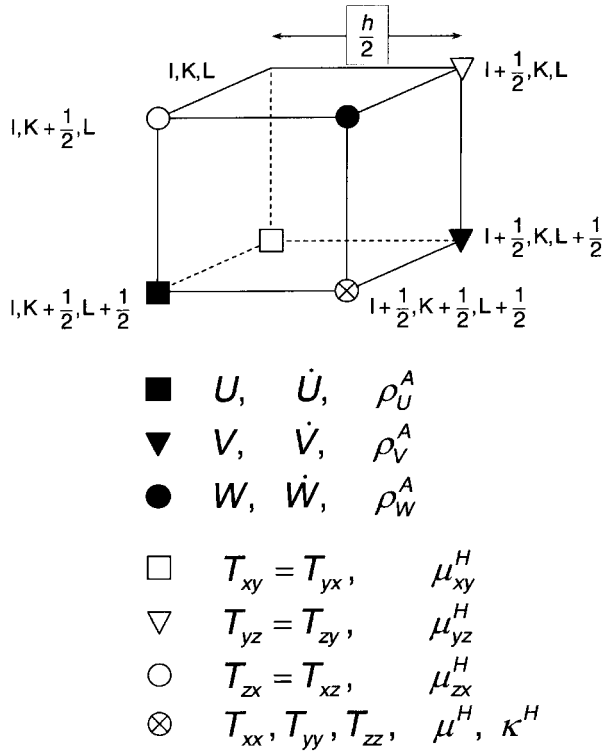

Figure 1. A staggered-grid FD cell with positions of the wave-field variables (displacement and/or particle-velocity components and stress-tensor components) and material parameters (elastic bulk and shear moduli).

the "H formulation." In the second option, the free surface coincides with the horizontal grid plane going through positions of W, T_{zx}, and T_{zy} (W formulation).

It is clear from equations (1) and (2) and FD approximation (4) that if the displacement/particle-velocity and stress-tensor components at the free surface and depths $h/2$ and h are to be calculated according to the FD scheme for interior grid points, values of displacement/particle-velocity and stress-tensor components at heights $-h/2$, $-h$, and $-3h/2$ (that is, above the free surface) are required.

The technique suggested originally by Levander (1988) for the 2D *P-SV* fourth-order velocity-stress FD scheme can be called the "stress-imaging technique." The technique applies explicit boundary conditions to the stress-tensor components located at the free surface and uses imaged values for the stress-tensor components above the free surface assuming their antisymmetry about the free surface. The antisymmetry,

$$\tau_{z\eta}(-z) = -\tau_{z\eta}(z);\ \eta \in \{x,y,z\}, \tag{5}$$

ensures condition (3). Rodrigues (1993) developed a 3D eighth-order staggered-grid displacement-stress scheme and used the stress-imaging technique in the H formulation. He found that it is necessary to take 10–15 grid points per shortest wavelength to avoid a significant numerical dispersion. Therefore, he combined the stress-imaging technique with a vertically refined grid near the free surface and achieved good accuracy. Graves (1996) applied the stress-imaging technique in the H formulation in the 3D fourth-order velocity-stress modeling. He found the technique better than the vacuum-formulation approach, which applies the interior FD scheme to the free-surface grid points assuming zero density and elastic moduli above the free surface.

Gottschämmer and Olsen (2001) tested the accuracy of the H and W formulations in the 3D fourth-order staggered-grid velocity-stress modeling in a homogeneous half-space against the discrete-wavenumber (DWN) method. Applying "a Gaussian-shaped function corresponding to approximately 6 points per shear wavelength" (p. 619), they showed cases when one formulation is better than the other and vice versa. In conclusion, Gottschämmer and Olsen recommended the use of the W formulation and averaging across the free surface in order to obtain values of the horizontal components of the particle velocity at the free surface.

Kristek *et al.* (2002) performed detailed numerical accuracy tests of the H and W formulations of Levander's (1988) stress-imaging technique in the 3D fourth-order staggered-grid FD modeling. They showed that both formulations require at least 10 grid spacings per minimum wavelength ($\lambda_{\min}/h = 10$) if Rayleigh waves are to be propagated without significant grid dispersion in the range of epicentral distances up to $22\lambda_{\min}$. Because interior fourth-order staggered-grid schemes usually do not require sampling denser than $\lambda_{\min}/h = 6$ in the considered range of epicentral distances (Moczo *et al.*, 2000, 2002), an alternative technique (allowing $\lambda_{\min}/h = 6$) was desirable.

Kristek *et al.* (2002) developed a technique based on the adjusted FD approximations (AFDAs) and, applying the $\lambda_{\min}/h = 6$ spatial sampling, demonstrated its accuracy and efficiency by comparing it numerically with the DWN method. They also compared the AFDA technique to the combination of the W-formulation stress imaging with Rodrigues's (1993) vertically refined grid near the free surface. The numerical tests were performed for models of the homogeneous half-space and layer over half-space. The purpose of this article is to test the accuracy of the AFDA technique in models with lateral material discontinuities.

AFDA Technique

The principle of the technique (Kristek *et al.*, 2002) is simple. The technique uses the adjusted FD schemes to calculate displacement/particle-velocity and stress-tensor components at the free surface and depths $h/2$ and h. No virtual displacement/particle-velocity and stress-tensor values above the free surface are used, that is, no stress imaging is applied. The technique applies (1) directly prescribed zero values of τ_{zz} at the free surface in the H formulation or τ_{zx} and τ_{zy} in the W formulation and (2) AFDAs to the z derivatives at the grid points at the free surface and depths $h/2$

and *h.* The H-AFDA and W-AFDA are illustrated in Figure 2. Kristek *et al.* (2002) showed that while H-AFDA gives slightly better phases, W-AFDA gives better amplitudes. They concluded with the recommendation to use W-AFDA for the earthquake ground-motion modeling. The calculation of the stress-tensor and displacement components in W-AFDA is briefly summarized in the Appendix.

Effective Material Parameters at the Free Surface

Moczo *et al.* (2002) developed a heterogeneous 3D fourth-order staggered-grid FD scheme with volume harmonic averaging of the bulk and shear moduli and volume arithmetic averaging of density, and they demonstrated a very good level of accuracy of the scheme. The scheme enables an arbitrary position of the discontinuity in the spatial grid and thus accounts for a difference in a layer thickness smaller than the spatial grid spacing. Moczo *et al.* (2002) demonstrated that such a thickness variation can yield considerably different seismic motion. While the structure of the scheme is the same as that of standard fourth-order staggered-grid FD schemes, the difference is in the definition of the grid material parameters. With reference to Figure 1, volume arithmetic average of density and volume harmonic averages of elastic moduli are evaluated as

$$\rho^{\mathrm{A}}_{\mathrm{W}} = \rho^{\mathrm{A}}_{I+\frac{1}{2},K+\frac{1}{2},L} = \frac{1}{h^3}\int_{x_I}^{x_{I+1}}\int_{y_K}^{y_{K+1}}\int_{z_{L-1/2}}^{z_{L+1/2}} \rho\, dx\, dy\, dz, \tag{6}$$

$$\mu^{\mathrm{H}}_{zx} = \mu^{\mathrm{H}}_{I,\,K+\frac{1}{2},L} = \left[\frac{1}{h^3}\int_{x_{I-1/2}}^{x_{I+1/2}}\int_{y_K}^{y_{K+1}}\int_{z_{L-1/2}}^{z_{L+1/2}} \frac{1}{\mu}\, dx\, dy\, dz\right]^{-1}, \tag{7}$$

$$\mu^{\mathrm{H}}_{yz} = \mu^{\mathrm{H}}_{I+\frac{1}{2},K,L} = \left[\frac{1}{h^3}\int_{x_I}^{x_{I+1}}\int_{y_{K-1/2}}^{y_{K+1/2}}\int_{z_{L-1/2}}^{z_{L+1/2}} \frac{1}{\mu}\, dx\, dy\, dz\right]^{-1}, \tag{8}$$

and so on.

In the W formulation, displacement component W and stress-tensor components τ_{zx} and τ_{yz} are located at the free surface. Therefore, in the W-AFDA technique we evaluate corresponding grid material parameters $\rho^{\mathrm{A}}_{\mathrm{W}}$, μ^{H}_{zx}, and μ^{H}_{yz} as integral averages in the half grid-cell volumes (that is, we do not account for the upper half of the volume, which is located above the free surface):

$$\rho^{\mathrm{A}}_{\mathrm{W}} = \rho^{\mathrm{A}}_{I+\frac{1}{2},K+\frac{1}{2},0} = \frac{2}{h^3}\int_{x_I}^{x_{I+1}}\int_{y_K}^{y_{K+1}}\int_{z_0}^{z_{1/2}} \rho\, dx\, dy\, dz, \tag{9}$$

$$\mu^{\mathrm{H}}_{zx} = \mu^{\mathrm{H}}_{I,K+\frac{1}{2},0} = \left[\frac{2}{h^3}\int_{x_{I-1/2}}^{x_{I+1/2}}\int_{y_K}^{y_{K+1}}\int_{z_0}^{z_{1/2}} \frac{1}{\mu}\, dx\, dy\, dz\right]^{-1}, \tag{10}$$

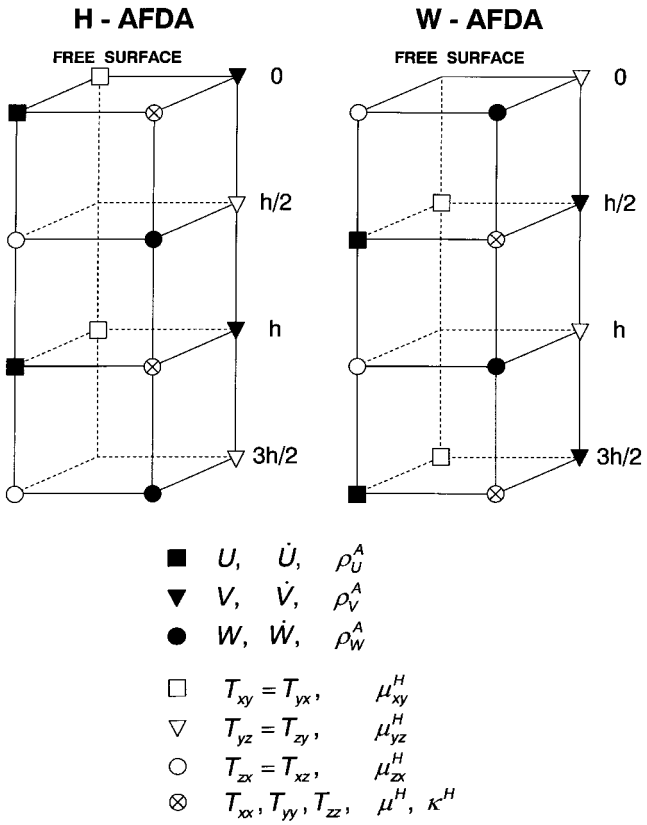

Figure 2. A part of the FD grid and position of the free surface in the H formulation (left) and W formulation (right) of the AFDA technique. The z derivatives at the grid points at the free surface and depths $h/2$ and h are calculated using adjusted FD approximations (given in the Appendix).

$$\mu^{\mathrm{H}}_{yz} = \mu^{\mathrm{H}}_{I+\frac{1}{2},K,0} = \left[\frac{2}{h^3}\int_{x_I}^{x_{I+1}}\int_{y_{K-1/2}}^{y_{K+1/2}}\int_{z_0}^{z_{1/2}} \frac{1}{\mu}\, dx\, dy\, dz\right]^{-1}. \tag{11}$$

Test Examples

Numerical tests of the technique against the DWN method for the homogeneous half-space and single layer over half-space have been presented in papers by Kristek *et al.* (2002) and Moczo *et al.* (2002). Because local surface geologic conditions, which strongly affect the earthquake ground motion, often include distinct lateral material discontinuities that reach the free surface, it is important to test the AFDA technique against an independent method that is capable of accounting for such a medium heterogeneity with sufficient accuracy. We considered models with vertical and oblique material discontinuities reaching the planar free surface and calculated synthetic seismograms by the FD method with the AFDA technique (Kristek *et al.*, 2002; Moczo *et al.*, 2002) and standard finite-element (FE) method. We chose the FE method to test our FD modeling because boundary conditions at the free surface and at internal material discontinuities are naturally and well satisfied in the FE method.

Figure 3 shows two models, A and B, of soft rectangular and parallelogram-shaped inclusions embedded in harder basements. Both inclusions are infinitely long in the direction of the y axis (perpendicular to the plane of the vertical cross section shown in the figure). Relatively deep inclusions were chosen in order to enhance the role of the contact of the inclusion–basement interface with the free surface in forming the surface motion. In order to test the capability of our FD modeling to account for different positions of the same physical inclusion in the spatial grid, we performed four different FD calculations for the same physical inclusion and the same physical problem, that is, four FD calculations for model A and four FD calculations for model B. Figure 4 indicates four different positions (a, b, c, and d) of the model A and model B inclusions in the spatial grids. Because the physical source–inclusion distance (in the x axis direction) is the same in all four configurations, the grid spacings in the four grids are slightly different (100.000, 102.128, 104.348, and 106.667 m in grids a, b, c, and d, respectively).

The source was a vertical body force acting at one point (grid position of the w component of displacement) at the free surface. Its source time function was a Gabor signal, $s(t) = \exp\{-[\omega(t - t_s)/\gamma]^2\}\cos[\omega(t - t_s) + \theta]$; $\omega = 2\pi f_p$, $t \in \langle 0,2t_s\rangle$, with predominant frequency $f_p = 0.225$ Hz, $\gamma = 1.5$, phase shift $\theta = 1.5708$, and $t_s = 4.0$ sec.

Before we compare FD synthetics against the FE synthetics at selected receiver positions, we can look at the FD synthetics calculated for configuration a of both models A and B. Figure 5 shows three components of displacement at 44 receiver positions at the free surface along a profile parallel to the x axis. If the grid coordinates of the source are $(I_s,K_s,0)$, then the leftmost receiver in the profile (numbered 1) has grid coordinates $(I_s + 6, K_s + 36,0)$. The grid coordinates of the rightmost receiver in the profile are $(I_s + 49, K_s + 36,0)$. The distance between two neighboring receivers is equal to one grid spacing, which is 100 m in configuration a. It is clear from Figure 5 that the two geometries of the soft inclusions produce considerably different motions, especially within the inclusions. The difference between the motions justifies the use of the two models and chosen frequency range (up to 1 Hz) for testing the sensitivity of the FD modeling to variation in the geometry of lateral discontinuities reaching the free surface.

For comparison between the FD and FE synthetics, we selected three receivers along the profile: looking in the positive x-axis direction, one receiver is in front of the inclusion (labeled 1), one is within the inclusion (2), and one is behind the inclusion (3). Grid coordinates, the same in all four grids, are $(I_s + 6, K_s + 36,0)$, $(I_s + 15, K_s + 36,0)$, and $(I_s + 24, K_s + 36,0)$ for receivers 1, 2, and 3, respectively. Because the sizes of the grid spacings in the four grids are slightly different, these grid coordinates mean slightly different physical positions of each of the three receivers in the each of the a, b, c, and d calculations. The actual receiver coordinates are given in Table 1. The time step used in all eight FD calculations was 0.014 sec.

For comparison, we performed one (much more computer-time- and memory-consuming) FE calculation for model A and one FE calculation for model B. A standard second-order accurate displacement formulation of the FE method was used to calculate the FE synthetics. The FE mesh inside the inclusion in model A was made of cubes with an edge size of 50 m. Rectangular parallelepipeds were used outside the inclusion. The FE mesh for model B was made of parallelepipeds such that the geometry of the inclusion was strictly followed. The parallelepipeds were obtained by deformation of the elements used in model A. The time step

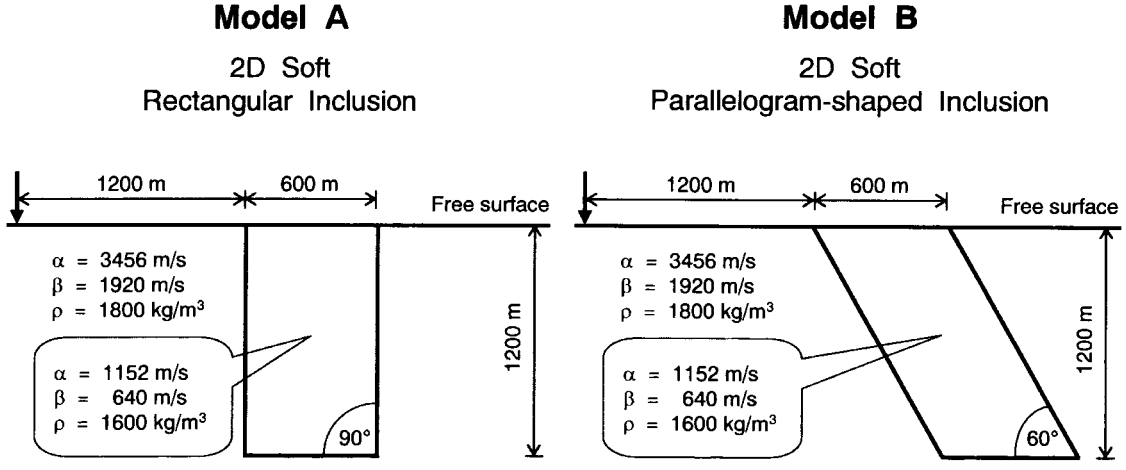

Figure 3. Vertical xz cross sections of models A and B and mechanical parameters of the models. Model A: a soft rectangular inclusion; model B: a soft parallelogram-shaped inclusion. The inclusions are infinitely long in the direction of the y axis perpendicular to the plane of the vertical cross section. The arrows (left) show positions of the vertical body forces acting as point sources. α, P-wave velocity; β, S-wave velocity; ρ, density.

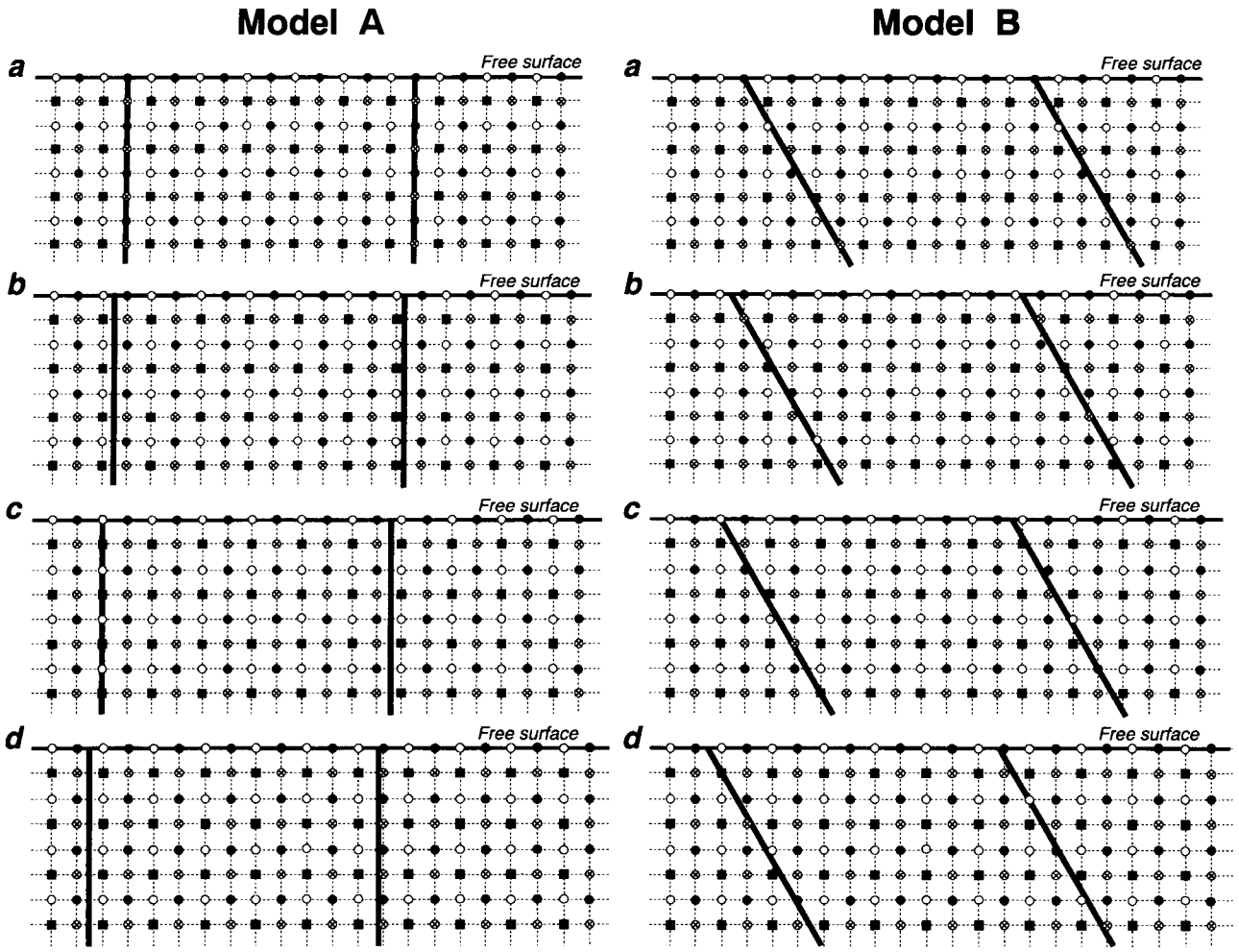

Figure 4. Left: Positions of the soft rectangular inclusion (model A) in the spatial grids in four (a, b, c, and d) FD calculations for the same inclusion, indicated in one vertical grid plane. The meaning of the symbols is the same as in Figures 1 and 2. Grid spacings in grids a, b, c, and d are 100, 102.128, 104.348, and 106.667 m, respectively. Slightly different grid spacings are used in order to have different positions of the same physical inclusion with respect to the spatial grid and, at the same time, to have physically the same source–inclusion configuration in all four calculations. Right: The same, but for model B.

used in both FE calculations was the same as in all FD calculations.

The FE displacement values at exact positions of the FD receivers were calculated from displacement values at FE nodes simply using the element shape functions.

The FD and FE synthetics for the three selected receiver positions are shown in Figure 6. Given the fact that both methods are just approximate and that the models are strongly laterally heterogeneous, the overall agreement between the FE and FD synthetics is very good. The largest difference can be seen on the w component of receiver 2 in grid configuration d for model A. A possible explanation for this particular difference might be the fact that the physical interface is too close but not exactly on the vertical grid plane. The synthetics for configurations a, b, c, and d also show that the FD scheme is capable to see the same physical model regardless of its position in the spatial FD grid.

We also compared the FD and FE synthetics for other profiles going through the inclusions. We did not see a difference between the FD and FE synthetics larger than that mentioned earlier. In fact, the differences were all smaller.

We think that our numerical tests show that our FD modeling, and particularly the AFDA technique for simulating the planar free surface, is sufficiently accurate and thus applicable to models with near-surface lateral discontinuities.

Conclusions

We numerically tested the accuracy of the AFDA technique in models with lateral material discontinuities reaching

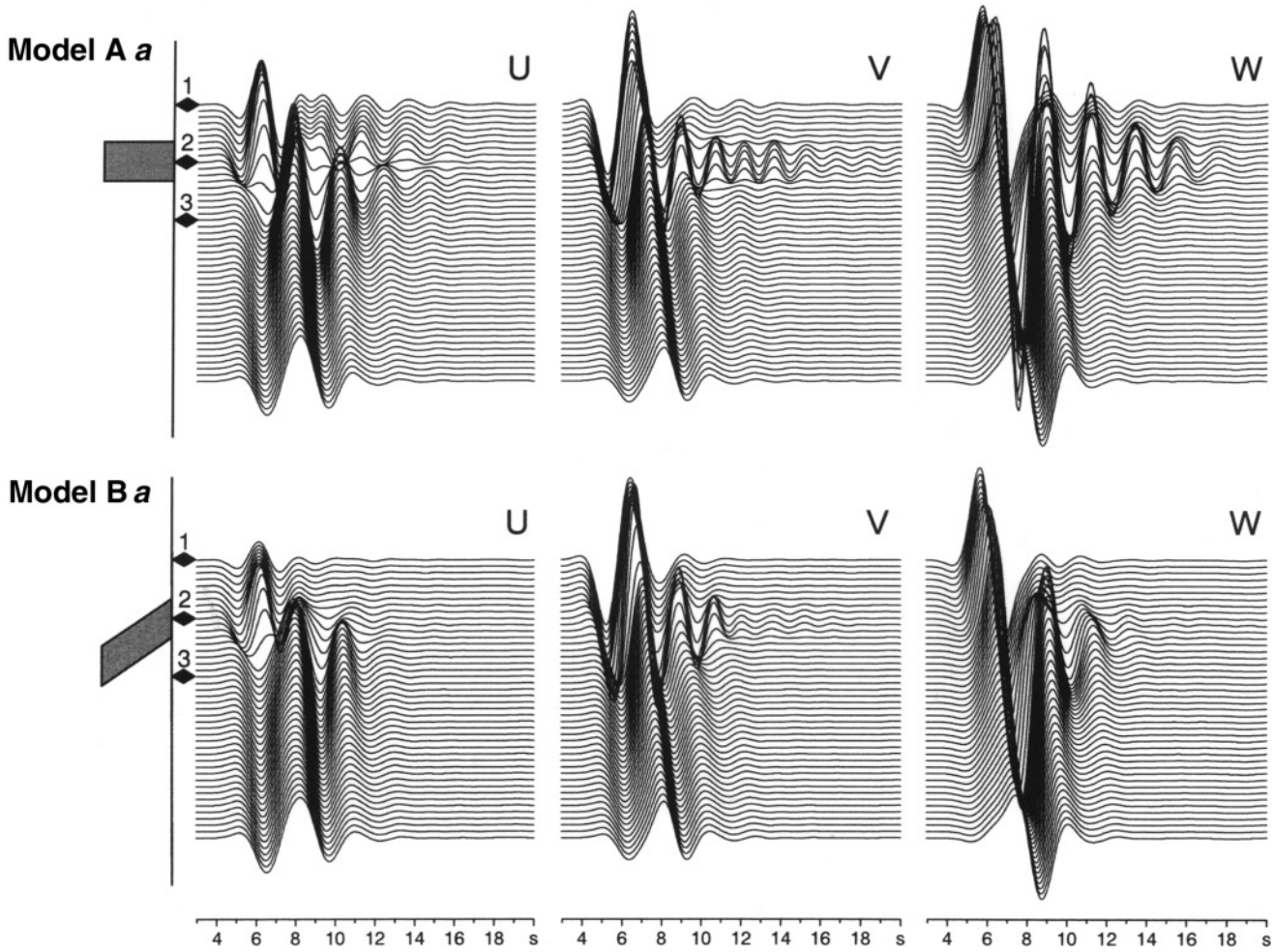

Figure 5. FD synthetics for receiver positions along a profile parallel to the x axis (perpendicular to the inclusion). The grid coordinates of the receivers in the y- and z-axis directions are $K_S + 36$ and 0, respectively, where K_S is the grid coordinate of the source. "a" denotes one of the four model-grid configurations. U, V, and W are Cartesian components of the displacement vector. Diamonds with numbers indicate selected receiver positions for which FD synthetics are compared with the FE synthetics (Fig. 6).

the free surface. For each of two physical models of soft inclusions embedded in the half-space, we considered four different positions of the inclusion in the spatial grid. We compared our FD synthetics with synthetics calculated by the standard FE method. The FE method was used because, unlike the FD method, it naturally and sufficiently accurately satisfies boundary conditions at the free surface and at internal material discontinuities. The comparison showed (1) the good accuracy of the AFDA technique in simulating the planar free surface and (2) the good sensitivity of our FD modeling to different positions of the same physical model in the spatial FD grid.

The implication of our study is that the AFDA technique can be used for simulating the planar free surface in models with lateral material discontinuities, which is the case for realistic models of surface sedimentary structures.

Acknowledgments

This work was supported in part by Grant No. 1/1090/21, VEGA, Slovak Republic, and European Commission Projects No. EVG1-CT-2000-00026 SESAME and EVG1-CT-2001-00040 EUROSEISRISK. The authors thank Jacobo Bielak for useful comments.

References

Gottschämmer, E., and K. B. Olsen (2001). Accuracy of the explicit planar free-surface boundary condition implemented in a fourth-order staggered-grid velocity-stress finite-difference scheme, *Bull. Seism. Soc. Am.* **91,** 617–623.

Graves, R. W. (1996). Simulating seismic wave propagation in 3D elastic media using staggered-grid finite differences, *Bull. Seism. Soc. Am.* **86,** 1091–1106.

Kristek, J., P. Moczo, and R. J. Archuleta (2002). Efficient methods to simulate planar free surface in the 3D fourth-order staggered-grid finite-difference schemes, *Studia Geophys. Geodet.* **46,** 355–381.

Levander, A. (1988). Fourth-order finite-difference *P-SV* seismograms, *Geophysics* **53,** 1425–1436.

Moczo, P., J. Kristek, and L. Halada (2000). 3D fourth-order staggered-grid finite-difference schemes: stability and grid dispersion, *Bull. Seim. Soc. Am.* **90,** 587–603.

Moczo, P., J. Kristek, V. Vavryčuk, R. J. Archuleta, and L. Halada (2002). 3D heterogeneous staggered-grid finite-difference modeling of seismic motion with volume harmonic and arithmetic averaging of elastic moduli and densities, *Bull. Seism. Soc. Am.* **92,** 3042–3066.

Rodrigues, D. (1993). Large-scale modeling of seismic wave propagation, *Ph.D. Thesis*, Ecole Centrale Paris.

Appendix

Summary of the Treatment of the Stress-Tensor and Displacement Components in the W-AFDA Technique

$T_{zx}(0) = 0$, $T_{zy}(0) = 0$.

$T_{xx}(h/2)$ is obtained from the fourth-order FD approximation to Hooke's law for τ_{xx}; derivative $w_{,z}$ is approximated by formula (A2).

$T_{yy}(h/2)$ and $T_{zz}(h/2)$: similar to $T_{xx}(h/2)$.

$T_{zx}(h)$ is obtained from the fourth-order FD approximation to Hooke's law for τ_{zx}; derivative $u_{,z}$ is approximated by formula (A3), in which $u_{,z}(0)$ is replaced by $w_{,x}$ due to condition $\tau_{zx}(0) = 0$.

$T_{zy}(h)$ is obtained from the fourth-order FD approximation to Hooke's law for τ_{zy}; derivative $v_{,z}$ is approximated by formula (A3), in which $v_{,z}(0)$ is replaced by $w_{,y}$ due to condition $\tau_{zy}(0) = 0$.

$W(0)$ is obtained from the fourth-order FD approximation to the equation of motion for w; derivative $\tau_{zz,z}$ is approximated by formula (A1), in which condition $\tau_{zz}(0) = 0$ is used.

$U(h/2)$ is obtained from the fourth-order FD approximation to the equation of motion for u; derivative $\tau_{zx,z}$ is approximated by formula (A2).

$V(h/2)$ is obtained from the fourth-order FD approximation to the equation of motion for v; derivative $\tau_{zy,z}$ is approximated by formula (A2).

$W(h)$ is obtained from the fourth-order FD approximation to the equation of motion for w; derivative $\tau_{zz,z}$ is approximated by formula (A4), in which condition $\tau_{zz}(0) = 0$ is used.

$$\varphi'(z_0) = \frac{1}{h}\left[-\frac{352}{105}\varphi(z_0) + \frac{35}{8}\varphi\left(z_0 + \frac{h}{2}\right) - \frac{35}{24}\varphi\left(z_0 + \frac{3}{2}h\right) + \frac{21}{40}\varphi\left(z_0 + \frac{5}{2}h\right) - \frac{5}{56}\varphi\left(z_0 + \frac{7}{2}h\right)\right] + O(h^4) \tag{A1}$$

$$\varphi'(z_0) = \frac{1}{h}\left[-\frac{11}{12}\varphi\left(z_0 - \frac{h}{2}\right) + \frac{17}{24}\varphi\left(z_0 + \frac{h}{2}\right) + \frac{3}{8}\varphi\left(z_0 + \frac{3}{2}h\right) - \frac{5}{24}\varphi\left(z_0 + \frac{5}{2}h\right) + \frac{1}{24}\varphi\left(z_0 + \frac{7}{2}h\right)\right] + O(h^4) \tag{A2}$$

$$\varphi'(z_0) = \frac{1}{h}\left[-\frac{h}{22}\varphi'(z_0 - h) - \frac{577}{528}\varphi\left(z_0 - \frac{h}{2}\right) + \frac{201}{176}\varphi\left(z_0 + \frac{h}{2}\right) - \frac{9}{176}\varphi\left(z_0 + \frac{3}{2}h\right) + \frac{1}{528}\varphi\left(z_0 + \frac{5}{2}h\right)\right] + O(h^4) \tag{A3}$$

$$\varphi'(z_0) = \frac{1}{h}\left[\frac{16}{105}\varphi(z_0 - h) - \frac{31}{24}\varphi\left(z_0 - \frac{h}{2}\right) + \frac{29}{24}\varphi\left(z_0 + \frac{h}{2}\right) - \frac{3}{40}\varphi\left(z_0 + \frac{3}{2}h\right) + \frac{1}{168}\varphi\left(z_0 + \frac{5}{2}h\right)\right] + O(h^4) \tag{A4}$$

Table 1
Relative Coordinates of the Three Receiver Positions

Rec.	Con.	Com.	Position of receiver x	y	z
1	a	U	550.000	3600.000	50.000
		V	600.000	3550.000	50.000
		W	600.000	3600.000	0.000
	b	U	561.704	3676.608	51.064
		V	612.768	3625.544	51.064
		W	612.768	3676.608	0.000
	c	U	573.914	3756.528	52.174
		V	626.088	3704.354	52.174
		W	626.088	3756.528	0.000
	d	U	586.669	3840.012	53.334
		V	640.002	3786.679	53.334
		W	640.002	3840.012	0.000
2	a	U	1450.000	3600.000	50.000
		V	1500.000	3550.000	50.000
		W	1500.000	3600.000	0.000
	b	U	1480.856	3676.608	51.064
		V	1531.920	3625.544	51.064
		W	1531.920	3676.608	0.000
	c	U	1513.046	3756.528	52.174
		V	1565.220	3704.354	52.174
		W	1565.220	3756.528	0.000
	d	U	1546.672	3840.012	53.334
		V	1600.005	3786.679	53.334
		W	1600.005	3840.012	0.000
3	a	U	2350.000	3600.000	50.000
		V	2400.000	3550.000	50.000
		W	2400.000	3600.000	0.000
	b	U	2400.008	3676.608	51.064
		V	2451.072	3625.544	51.064
		W	2451.072	3676.608	0.000
	c	U	2452.178	3756.528	52.174
		V	2504.352	3704.354	52.174
		W	2504.352	3756.528	0.000
	d	U	2506.675	3840.012	53.334
		V	2560.008	3786.679	53.334
		W	2560.008	3840.012	0.000

Actual relative coordinates of the three receiver positions in meters in grids a, b, c, and d assuming that the coordinates of the source are (0,0,0).

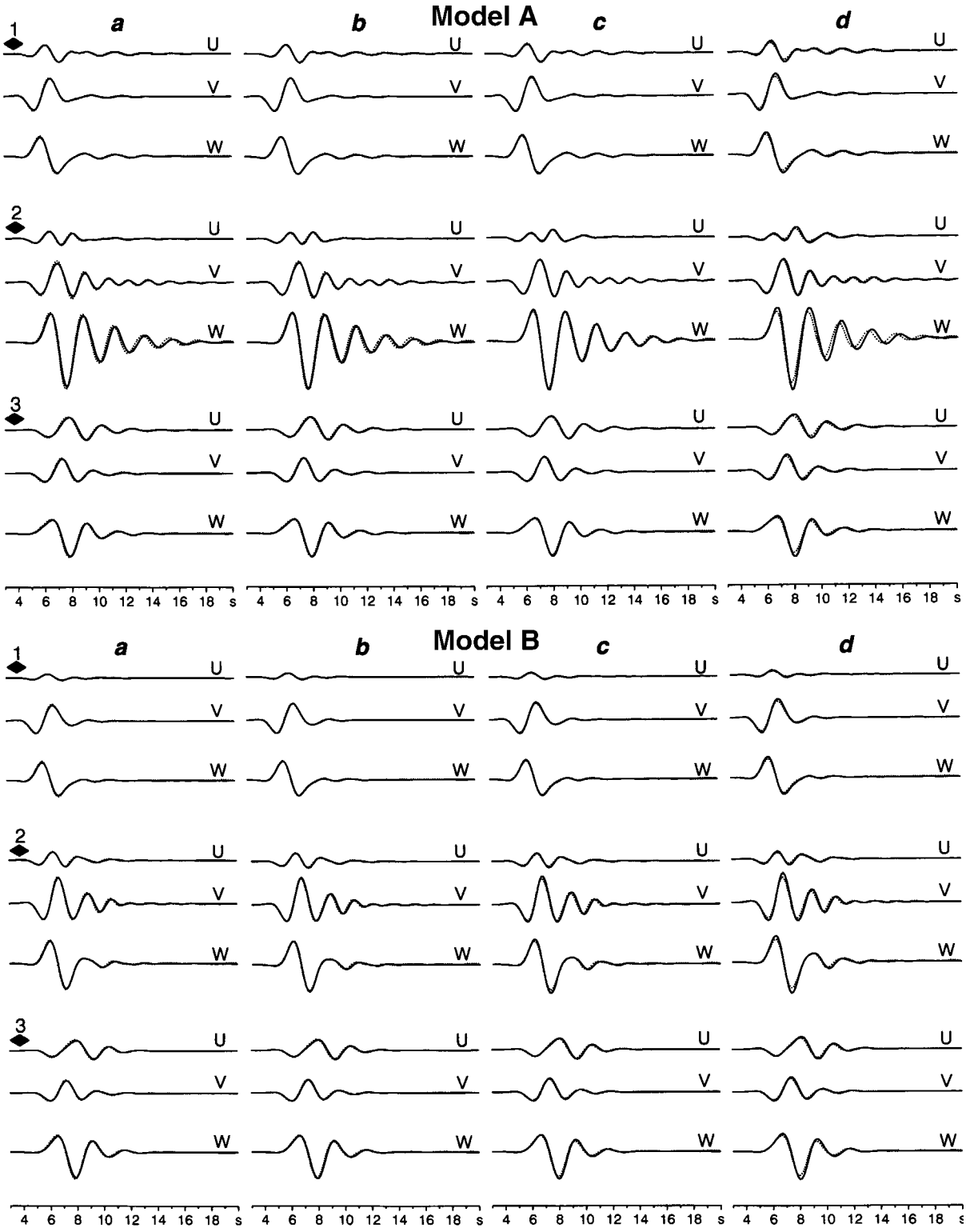

Figure 6. Comparison of the FD and FE synthetics for selected surface receiver positions along the profile parallel to the *x* axis. Looking in the positive *x*-axis direction, receiver 1 is in front of the inclusion, receiver 2 is approximately in the center of the inclusion, and receiver 3 is behind the inclusion. A and B refer to the models (Fig. 3); lowercase a, b, c, and d refer to four different model-grid configurations (Fig. 4). U, V, and W are Cartesian components of the displacement vector. FD = solid line, FE = dashed line.

Department of Physics of the Earth and Planets
Faculty of Mathematics, Physics, and Informatics
Comenius University
Mlynská dolina F1
842 48 Bratislava, Slovak Republic
(P.M., M.G.)

Geophysical Institute
Slovak Academy of Sciences
Dúbravská cesta 9
845 28 Bratislava,
Slovak Republic
(J.K.)

Manuscript received 12 March 2003.